Polymer Journal (2018) 50:671–678
https://doi.org/10.1038/s41428-018-0065-3

FOCUS REVIEW

Self-assembly of liquid-crystalline block copolymers in thin films: control of microdomain orientation

Xiaoxiong Zheng[1,2] · Yongbin Zhao[3] · Aihua Chen[1,2]

Received: 15 January 2018 / Revised: 8 April 2018 / Accepted: 9 April 2018 / Published online: 10 May 2018

Abstract

Block copolymer (BCP) lithography, as one of the most promising techniques for the next-generation integrated circuits, has been extensively investigated in recent years. Among the diverse types of BCPs, liquid-crystalline BCPs (LC-BCPs) formed by incorporating LC moieties into the BCPs have become increasingly attractive because of the tunable alignment of the LC chains. This review highlights the control of the microdomain orientation of PEO-*b*-PMA(Az) thin films via novel and convenient processing methods, including micropore extrusion and the introduction of polydimethylsiloxane (PDMS). Meanwhile, the mechanisms of the microdomain alignment transition are clarified and are closely related to the soft shearing field and the change in the block surface energy. Furthermore, some new perspectives for future research on the self-assembly of LC-BCP thin films are outlined from the point of view of material design, orientation control, and technological innovation.

Introduction

Block copolymers (BCPs), composed of chemically dissimilar polymer segments, can self-assemble into various ordered nanostructures with feature sizes on the scale of 5–100 nm. The size and morphology of the nanopatterns are readily tunable by changing the molecular weight and composition of the BCP. Meanwhile, orderly self-assembled thin films are required in many applications. For instance, in the fields of integrated circuits, high-density storage, and so forth, these BCP thin films have attracted enormous research interest as templates for novel nanolithography techniques [1–4]. To integrate BCP lithography into current industrial-scale production, several major challenges, including microdomain orientation control, processing accuracy, annealing time, and cost management, should be addressed [5, 6]. With regard to the aforementioned challenges, recent research has concentrated on directing the orientation of the self-assembly in BCP films, for instance, through the use of graphoepitaxy [7, 8], chemical prepatterning [9, 10], external fields [11, 12], etc. In comparison to the use of conventional amorphous–amorphous BCPs for the above techniques, the introduction of crystalline or liquid-crystalline (LC) segments into BCPs is a significant approach to fabricating microphase-separated nanostructures. In particular, LC-BCPs have been of interest because the LC components can be facilely oriented by external fields, such as electric or shearing fields [13, 14].

The combination of LC groups and BCPs is not only an effective means to achieve the transition to microdomain alignment but is also of scientific interest to understand the effect of two blocks' surface energy on the segregated domain morphology [15]. The synthesis of various LC chain structures, such as LC main chain, rod coil, and LC side chain, has been reported [16]. While it is extremely difficult to polymerize LC main-chain BCPs with a perfect structure, LC side-chain BCPs have been readily synthesized by living polymerization techniques [17]. Therefore, investigations of LC side-chain BCPs can assist us in understanding the precise correlation between BCP microphase segregation and LC alignment [18]. When BCPs with a side-chain nematic LC polymer block and an amorphous block form a segregated domain, the amorphous domain

✉ Aihua Chen
chenaihua@buaa.edu.cn

[1] School of Materials Science and Engineering, Beihang University, No. 37 Xueyuan Road, Haidian District, Beijing 100191, China

[2] Beijing Advanced Innovation Centre for Biomedical Engineering, Beihang University, Beijing, China

[3] Shandong Oubo New Material Co Ltd. Dongying Part Economic Development Zone, Shangdong 257088, China

can be oriented along the nematic director. This phenomenon is due to the tendency of mesogens to arrange along the interface of the nematic phase, known as the anchoring effect [13]. When the LC side chains in BCPs form a smectic phase, the orientation mainly depends on the mobility of the mesogens. The main chain domains are aligned vertical to small spacer smectic layers, while for a long spacer system, the main chains are oriented parallel to the layer interface [19].

Among various LC components, azobenzene is one of the most popular chromophore units for light-responsive materials and can bring about photoalignment, a photo-induced phase transition and other interesting properties for azobenzene-containing polymers [20–22]. We have reported on a designed amphiphilic LC diblock copolymer, PEO-*b*-PMA(Az), consisting of hydrophilic poly(ethylene oxide) (PEO) and hydrophobic polymethacrylate bearing azobenzene mesogen side chains (PMA(Az)). Self-assembled thin films can be readily formed by spin-coating 1 ~ 3 wt% toluene solutions on various non-modified substrates, such as silicon wafers, mica, and polyethylene terephthalate, followed by annealing at 140 °C in vacuum for several hours [23, 24]. This BCP forms a highly ordered microphase-separated film with perpendicular hexagonally oriented cylindrical PEO domains surrounded by the PMA (Az) matrix having a smectic LC phase [25]. The PEO domains are oriented parallel to the smectic layers for a long undecyl spacer. The one-dimensional periodic structure of the smectic layers displays a high bending elasticity, leading to an extremely wide cylinder morphology window (8.3% < PEO volume fraction < 52%) in the BCP phase diagram [26]. The perpendicular orientation has been successfully transferred to the parallel one via various developing methods, for instance, a top-coating method [27], a rubbing technique [28], and a fast ultraviolet-light-directed method [29]. In addition, a series of metal/metalloid nanodot and nanorod arrays have been prepared via these BCP film templates due to their amphiphilic properties [30–32].

Considering applications in manufacturing integrated circuits and other lithography fields, simple and low-cost approaches to preparing orderly parallel orientations of nanomaterials are desirable. In this review, we mainly concentrate on the control of microdomain orientation in PEO-*b*-PMA(Az) thin films. Novel and convenient processing methods are discussed first, including micropore extrusion and introduction of polydimethylsiloxane (PDMS). Meanwhile, the mechanisms of the microdomain alignment transition are clarified, including their close relationships to the soft shearing field and the differences in block surface energy. Finally, we summarize key and

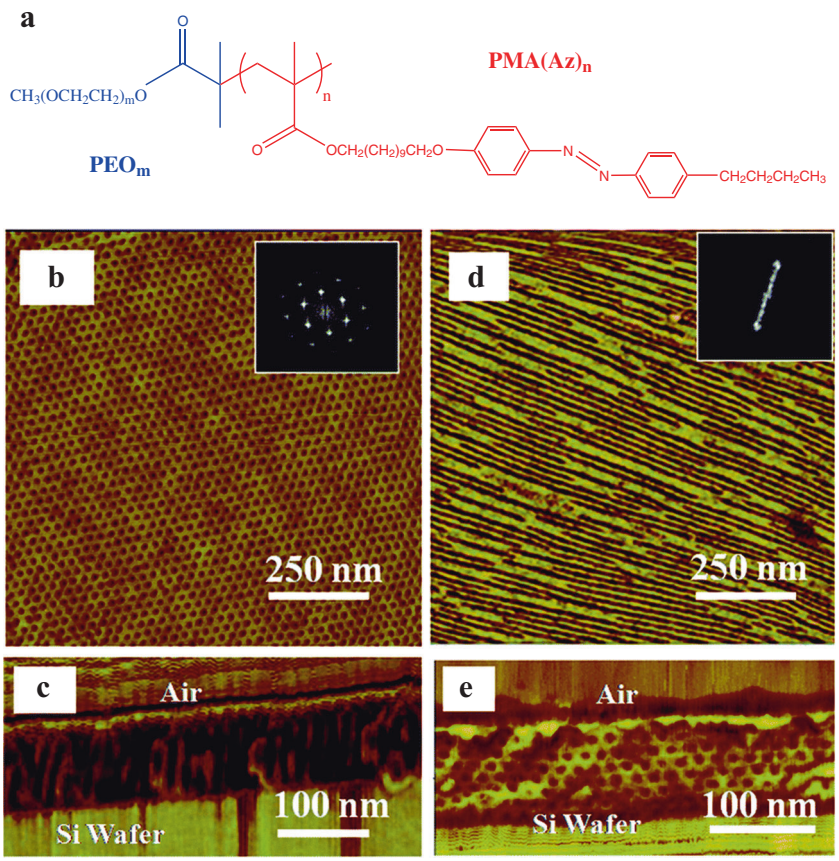

Fig. 1 Chemical structure of the PEO-*b*-PMA(Az) block copolymer (**a**) and typical AFM images of PEO_{114}-*b*-$PMA(Az)_{45}$ thin films subjected to the extrusion process or not (**b**–**e**). **b**, **c** Top-view and cross-section images of the perpendicular PEO cylindrical orientation without extrusion. **d**, **e** Top-view and cross-section AFM phase images of the BCP films subjected to the extrusion process. The insets in **b** and **d** show the corresponding fast Fourier transform images

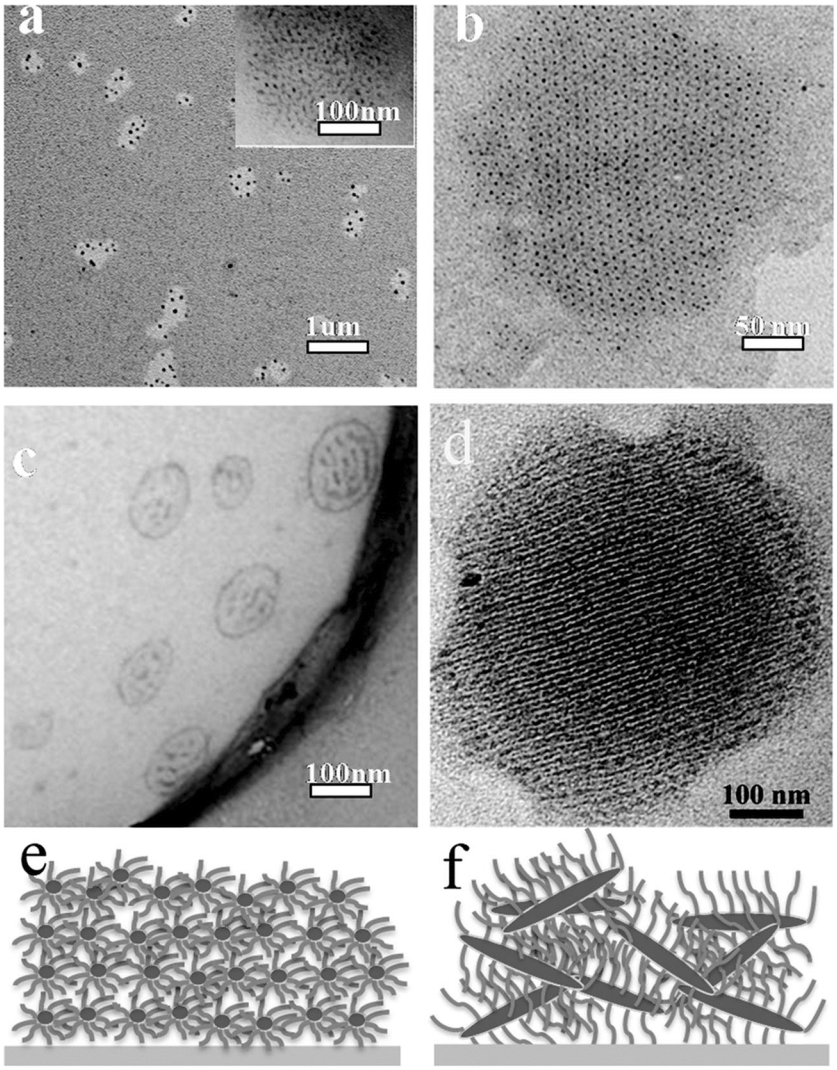

Fig. 2 TEM images of PEO-*b*-PMA(Az) thin films obtained by drop casting BCP toluene solutions of 0.04 wt% onto Cu grids. **a**, **c** BCP solutions without and with the extrusion process, respectively. **b**, **d** Samples annealed at 140 °C in vacuum for 2 h. Schemes of corresponding micelle aggregates (**e**, **f**)

emerging questions and provide an outlook for the future of LC-BCP thin films.

Results and discussion

Micropore extrusion-induced alignment transition

Recently, the utilization of shearing fields, one of the most popular approaches for aligning LC groups, has been realized to adjust or enhance the orientation of BCP films [33]. In our case, the microdomain orientation transition in PEO-*b*-PMA(Az) thin films has been achieved by a mechanical rubbing method [28]. Herein, we prepared parallel cylindrical domains from perpendicularly oriented ones through a simple extrusion process on a large scale [34].

For the extrusion process, a laboratorial syringe pump with polytetrafluoroethylene filters was employed to transfer BCP solutions to Si wafers or water surfaces. All the

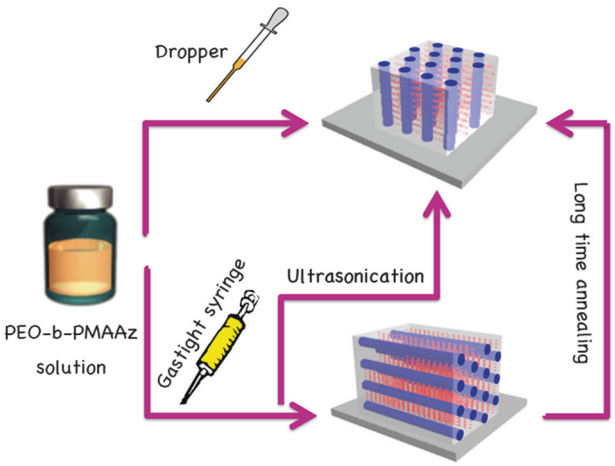

Fig. 3 The orientation transition from perpendicular to parallel alignments of PEO cylindrical domains of PEO-*b*-PMA(Az) films demonstrated by extruding BCP solutions through the micropore of a plastic gastight syringe. The parallelized orientation of PEO domains induced by this micropore extrusion can be recovered to the perpendicular alignment via ultrasonication of the extruded BCP solutions and subsequent annealing

film samples were annealed at 140 °C in vacuum for 2 h. Figure 1a shows the chemical structure of the PEO-*b*-PMA (Az) BCP. Figure 1b, c and Fig. 1d, e are typical atomic force microscopy height images of the top view and section view of PEO-*b*-PMA(Az) films on a Si wafer before and after being extruded by a gastight syringe, respectively. Highly ordered arrays of PEO cylindrical domains vertical to the substrate were obtained from the spin-coated BCP solutions after thermo-annealing, as shown in Fig. 1b, c. It is clear that the PEO cylindrical domains became parallel to the substrate after the micropore extrusion process, as shown in Fig. 1d. The morphology of the in-plane PEO domains with a hexagonally ordered alignment was further proven in the cross-section image of Fig. 1e.

To explore the effect of the extrusion process on the microdomain orientation, we prepared a diluted BCP toluene solution and observed the micelles by transmission electron microscope (TEM). Figure 2a, b shows that spherical BCP micelles formed large aggregations, and then, after annealing, hexagonally oriented block domains were observed consisting of PEO domains stained by RuO_4. With regard to the extruded BCP solution, Fig. 2c, d indicates that the spherical BCP micelles transformed to a rod-like shape and generated aligned PEO domains after annealing. Apparently, micropore extrusion can induce micelle morphology deformation. For the PMA(Az) block, the deformation cannot be released rapidly due to the rigid smectic LC phase and extrudate swell effect [35]. On the other hand, we concluded that a fast volatilizing solvent, such as toluene in this work, cooperates to maintain the rod-like micelle morphology and directs the final in-plane-aligned PEO cylinders, subject to thermal annealing, as shown in Fig. 2e, f. In addition, the deformation can be recovered through the disentanglement of molecular chains by methods such as ultrasonication or long-time annealing. Here we completely recovered the PEO cylindrical domains

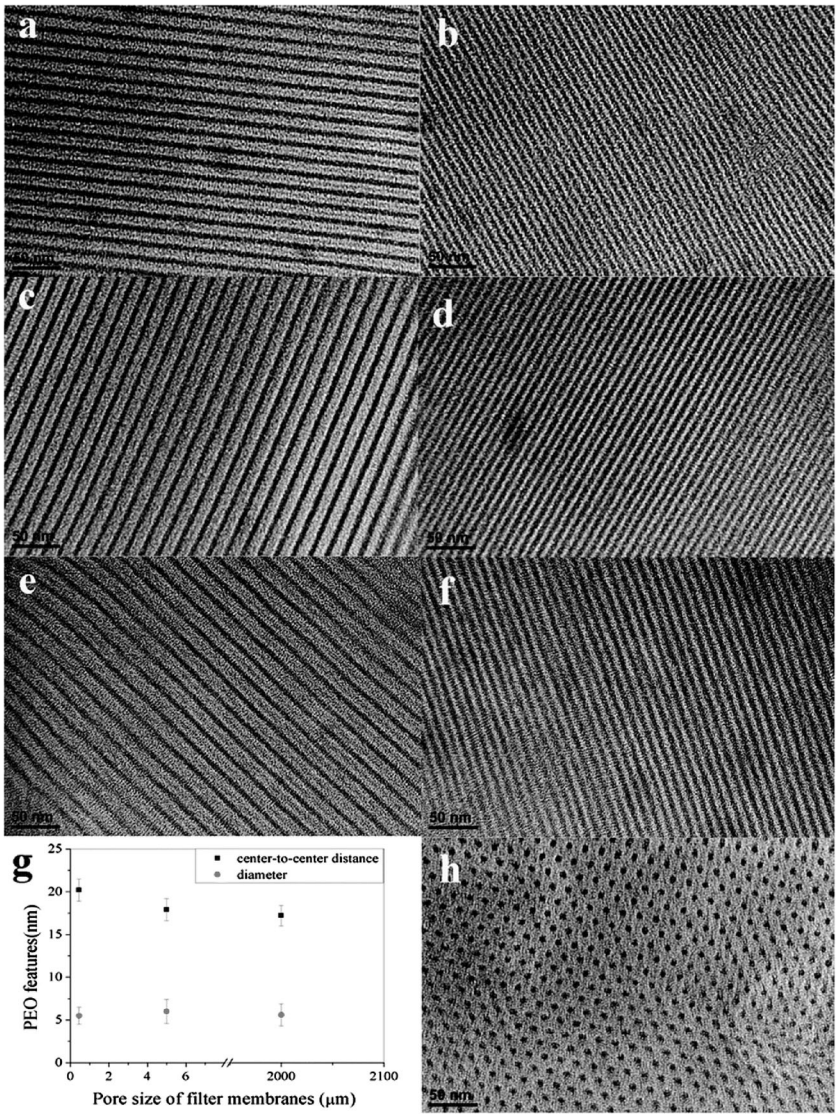

Fig. 4 TEM images of self-assembled PEO-*b*-PMA(Az) after micropore extrusion with filter membranes of different pore sizes: **a**, **b** no filter membrane; **c**, **d** 5 μm; and **e**, **f** 0.45 μm. **g** Plots of the pore size of the filter membrane versus the diameter and center-to-center distance of the PEO cylindrical domain and **h** without extrusion

(in-plane to out-of-plane alignment) via ultrasonication of the extruded BCP solution or thermal annealing of the as-placed solution for 5 days, as shown in Fig. 3. Furthermore, it is interesting that the extrudate swell effect, which is a common macroscopic phenomenon for the extrusion process, was also observed in this microphase separation system. As shown in Fig. 4, a smaller pore size contributed to the relatively larger periodicity of the PEO domains, indicating that the periodicity of the in-plane cylindrical PEO domains can be tuned by the pore size of the filter membrane. This method presents a versatile way to finely control the orientation and feature size of self-assembled BCP films without varying the molecular weight.

PDMS-assisted alignment transition

In the absence of other variables, the orientation of cylindrical microdomains within a BCP thin film generally depends on the difference of interfacial energies between both blocks and the substrate and the surface energies of the two blocks [36]. Some methods for orientation control have been mainly achieved by adjusting the interfacial energies, such as modifying substrates by random copolymer brushes [37] and coating with a polymer layer [38]. In our work, the orientation control of PEO-*b*-PMA(Az) has been realized by a PDMS top-coating method due to the ultra-low surface tension of PDMS [27]. Previous research has mainly concentrated on the soft shearing from different thermal expansion volumes between PDMS coatings and BCP films [27, 39]. However, a control method by adjusting surface energies has rarely been reported. Herein, we demonstrate another simple method to realize the orientation transition by introducing a small amount of PDMS into the BCP solution, followed by thermal annealing [40]. As shown in Fig. 5a, b, we prepared in-plane-aligned cylinders via the PDMS-assisted method. The dark stripes are PEO domains stained by RuO_4, and the gray regions correspond to the PMA(Az) matrix. It is noted that perpendicular cylinders are transited to in-plane cylinders to obtain two viewing directions—corresponding to the (10) and (11) planes of hexagonal alignment—forming narrow stripes and wide stripes, respectively, as shown in Fig. 5c. The feature sizes, such as cylinder diameter and stripe distance, were determined using the TEM images and correspond with the geometrical relationship shown in Fig. 5d.

To investigate the effect of PDMS on the alignment of LC-BCP films, the effect of the PDMS molecular weight was determined. Figure 6a–d shows TEM images of BCP films containing 0.5 wt% PDMS of different molecular weights. It is interesting to note that PEO cylinders maintained vertical alignment with a slight tilt after the introduction of low-molecular-weight PDMS ($M_{PDMS} = 1.25$ kg/mol), while with M_{PDMS} increased to 28 kg/mol, the mixed toluene solution of BCP and PDMS became inhomogeneous, forming visible macro-phase separation.

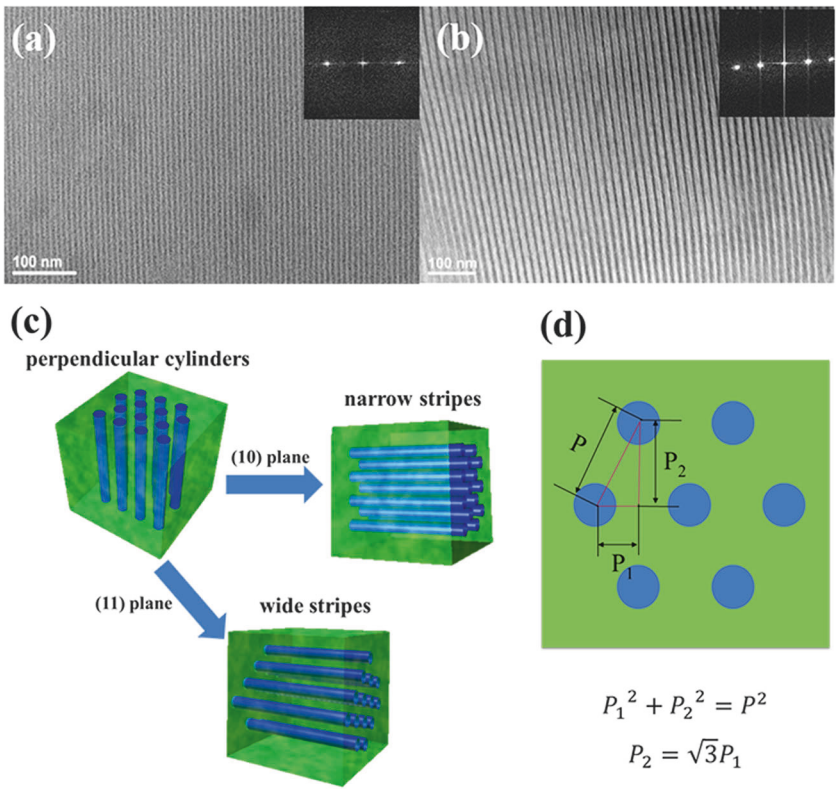

Fig. 5 **a**, **b** TEM images of the narrow and wide stripes of BCP films subjected to the PDMS-assisted ($M_{PDMS} = 13$ kg/mol, 0.5 wt%) process. The insets show the corresponding fast Fourier transform images. **c** Schematic representations of the orientation transition from perpendicular to parallel alignments of PEO cylindrical microdomains. **d** The geometrical relationship of perpendicular cylinders, narrow stripes, and wide stripes. P, P_1, and P_2 are the center-to-center distances of perpendicular cylinders, narrow stripes, and wide stripes, respectively

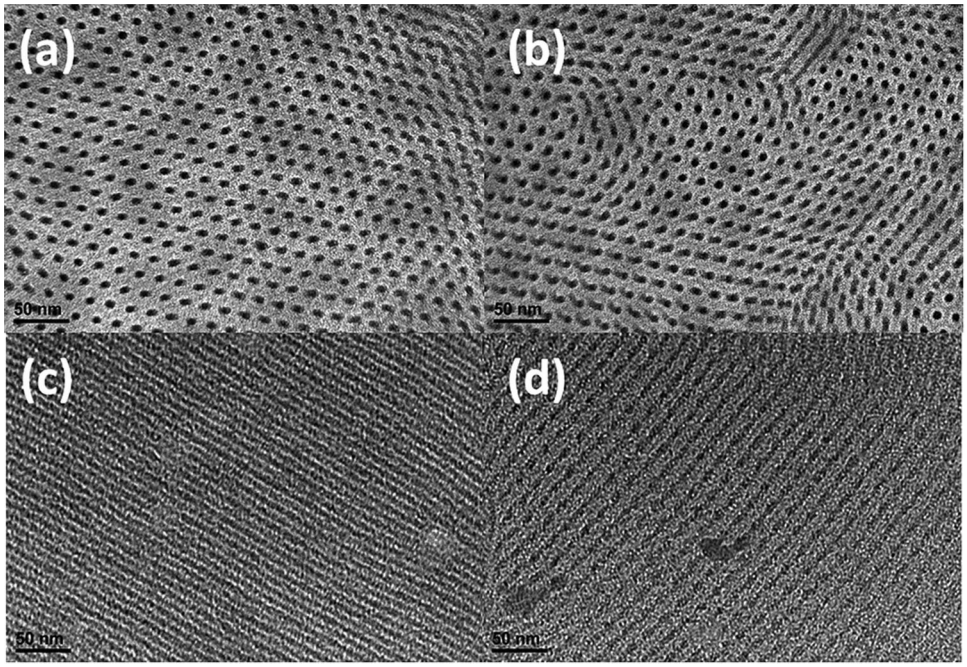

Fig. 6 TEM images of self-assembled PEO-*b*-PMA(Az) after the introduction process with PDMS (0.5 wt%) of different molecular weights: **a**, **b** 1.25 kg/mol; and **c**, **d** 28 kg/mol

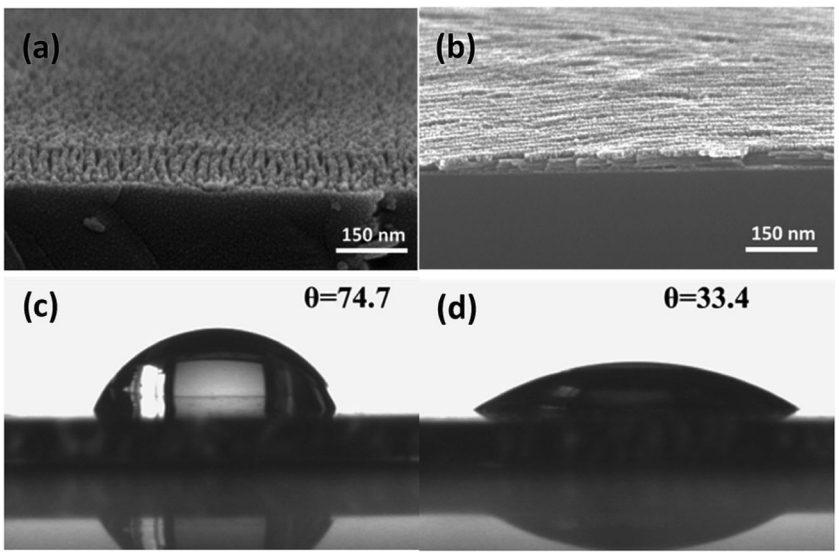

Fig. 7 **a** SEM image of vertically aligned SiO_2 nanorod arrays from PEO-*b*-PMA(Az) films. **b** An SEM image of SiO_2 nanowire arrays obtained from PEO-*b*-PMA(Az) films using the PDMS-assisted process. **c**, **d** Water contact angles of out-of-plane SiO_2 perpendicular nanorod arrays and in-plane SiO_2 nanowire arrays

As mentioned above, PDMS is well known for its ultra-low surface tension. In this work, we supposed that PDMS chains would adhere to the surface of PEO and PMA(Az) blocks because of the characteristics of PDMS. Therefore, it is reasonable that the surface energy difference between PEO and PMA(Az) blocks was changed to some extent due to the interference of PDMS. In addition, the soft shear force also existed in this system, coming from the different coefficients of thermal expansion of PDMS and the LC phase during the thermal annealing process. Considering these two factors, it can be proposed that the PEO domains can transfer to parallel alignment if PDMS provides sufficient effects upon completely surrounding the PEO domains, as shown in Fig. 5a, b, while in the case of partial envelopment by low-molecular-weight PDMS, PEO cylinders only inclined to a certain degree, as shown in Fig. 6a, b. It is possible to generalize this method for other LC-BCPs, broadening the applications of surface modification.

Pattern transformation from BCP templates

Previously, we prepared vertically oriented SiO_2 nanorod arrays from PEO-*b*-PMA(Az) films via the sol-gel method [30, 31], as shown in Fig. 7a. The feature sizes can be tuned

by BCP templates with different volume fractions of PEO domains. Here we demonstrate in-plane SiO_2 nanowire arrays achieved from both micropore extrusion-induced and PDMS-introduced BCP films, as shown in Fig. 7b. The hydrophilicities of SiO_2 were investigated by an automated contact angle tester, as shown in Fig. 7c, d. The water contact angle of the in-plane SiO_2 nanowire arrays was 33.4°, compared with the value of 74° for the out-of-plane SiO_2 perpendicular cylinders, which confirmed that the Si wafer substrates bearing in-plane SiO_2 nanowire arrays are more hydrophilic. This method can be expanded to other oxides, especially semiconductors, such as TiO_2 and Ta_2O_5. The hydrophilicity and morphology of nanostructured semiconductors can be readily tuned by BCP templates and processing methods, which facilitates the application in catalysis and integrated circuit fields.

Conclusions and outlook

In summary, we demonstrate the facile control of the microdomain orientation in LC-BCP thin films by means of micropore extrusion and the introduction of PDMS, instead of complicated processes or costly apparatus. We made the most of the mobility of the smectic LC phase and explored the effects of the soft shearing field and the surface energy difference on the LC segment alignment. In closing, here are some new perspectives for the future of LC-BCP thin-film research. First, more functional blocks can be combined with LC segments. For example, poly(4-vinylpyridine) has an extraordinary coordinating capability, which can be used to prepare noble metal or additional oxide nanostructures. Then, we may take advantage of the controllable LC domain orientation to prepare various patterns for catalysis or semiconductor purposes. Furthermore, smaller feature sizes of self-assembled BCP templates are significant for next-generation integrated circuits. Such sizes may be realized by designing a new BCP with a high Flory–Huggins interaction parameter or utilizing covalent bonds to strengthen the surface of two blocks. In addition, future work will continue on updated techniques to reduce domain defect densities to achieve near perfect order. Finally, it is attractive to research the relationship between the LC segment alignment and macroscopic material functions, such as light- or moisture-induced mechanical actuation. Further efforts in these areas will ultimately contribute to the design of novel nanomaterial systems for next-generation thin-film applications.

Acknowledgements This work was financially supported by the National Natural Science Foundation of China (Nos. 51272010 and 51472018), the Beijing Nova Program (No. XX2013009), and the Fundamental Research Funds for the Central Universities.

Compliance with ethical standards

Conflict of interest The authors declare that they have no conflict of interest.

References

1. Wu ML, Wang D, Wan LJ. Directed block copolymer self-assembly implemented via surface-embedded electrets. Nat Commun. 2016;7:10752.
2. Yoo HG, Byun M, Jeong CK, Lee KJ. Performance enhancement of electronic and energy devices via block copolymer self-assembly. Adv Mater. 2015;27:3982–98.
3. Li WH, Muller M. Directed self-assembly of block copolymers by chemical or topographical guiding patterns: optimizing molecular architecture, thin-film properties, and kinetics. Prog Polym Sci. 2016;54-55:47–75.
4. Michman E, Shenhar R. Directed self-assembly of block copolymer-based nanocomposites in thin films. Polym Advan Technol. 2017;28:613–22.
5. Ji SX, Wan L, Liu CC, Nealey PF. Directed self-assembly of block copolymers on chemical patterns: a platform for nanofabrication. Prog Polym Sci. 2016;54-55:76–127.
6. Kim S, Bates CM, Thio A, Cushen JD, Ellison CJ, Willson CG, Bates FS. Consequences of surface neutralization in diblock copolymer thin films. Acs Nano. 2013;7:9905–19.
7. Segalman RA, Yokoyama H, Kramer EJ. Graphoepitaxy of spherical domain block copolymer films. Adv Mater. 2001;13:1152–5.
8. Jeong SJ, Moon HS, Kim BH, Kim JY, Yu J, Lee S, Lee MG, Choi H, Kim SO. Ultralarge-area block copolymer lithography enabled by disposable photoresist prepatterning. Acs Nano. 2010;4:5181–6.
9. Kim SO, Solak HH, Stoykovich MP, Ferrier NJ, De Pablo JJ, Nealey PF. Epitaxial self-assembly of block copolymers on lithographically defined nanopatterned substrates. Nature. 2003;424:411–4.
10. Ruiz R, Kang H, Detcheverry FA, Dobisz E, Kercher DS, Albrecht TR, de Pablo JJ, Nealey PF. Density multiplication and improved lithography by directed block copolymer assembly. Science. 2008;321:936–9.
11. Ruppel M, Pester CW, Langner KM, Sevink GJ, Schoberth HG, Schmidt K, Urban VS, Mays JW, Boker A. Electric field induced selective disordering in lamellar block copolymers. Acs Nano. 2013;7:3854–67.
12. Kathrein CC, Bai W, Currivan-Incorvia JA, Liontos G, Ntetsikas K, Avgeropoulos A, Böker A, Tsarkova L, Ross CA. Combining graphoepitaxy and electric fields toward uniaxial alignment of solvent-annealed polystyrene–b–poly(dimethylsiloxane) block copolymers. Chem Mater. 2015;27:6890–8.
13. Tokita M, Adachi M, Masuyama S, Takazawa F, Watanabe J. Characteristic shear-flow orientation in LC block copolymer resulting from compromise between orientations of microcylinder and LC mesogen. Macromolecules. 2007;40:7276–82.
14. Hamley IW, Castelletto V, Lu ZB, Imrie CT, Itoh T, Al-Hussein M. Interplay between smectic ordering and microphase separation in a series of side-group liquid-crystal block copolymers. Macromolecules. 2004;37:4798–807.
15. Ishige R, Ohta N, Ogawa H, Tokita M, Takahara A. Fully liquid-crystalline ABA triblock copolymer of fluorinated side-chain liquid-crystalline A block and main-chain liquid-crystalline B block: higher order structure in bulk and thin film states. Macromolecules. 2016;49:6061–74.
16. Mao G, Ober CK. Block copolymers containing liquid crystalline segments. Acta Polym. 1997;48:405–22.

17. Figueiredo P, Gronski W, Bach M. Preparation of oriented liquid-crystalline/isotropic block copolymer films with parallel or perpendicular arrangement of smectic layers and lamellar microdomains. Macromol Rapid Commun. 2002;23:38–43.
18. Asaoka S, Uekusa T, Tokimori H, Komura M, Iyoda T, Yamada T, Yoshida H. Normally oriented cylindrical nanostructures in amphiphilic PEO–LC diblock copolymers films. Macromolecules. 2011;44:7645–58.
19. Anthamatten M, Zheng WY, Hammond PT. A morphological study of well-defined smectic side-chain LC block copolymers. Macromolecules. 1999;32:4838–48.
20. Lv JA, Liu Y, Wei J, Chen E, Qin L, Yu Y. Photocontrol of fluid slugs in liquid crystal polymer microactuators. Nature. 2016;537:179–84.
21. Liu Y, Xu B, Sun S, Wei J, Wu L, Yu Y. Humidity- and photo-induced mechanical actuation of cross-linked liquid crystal polymers. Adv Mater. 2017;29:1604792.
22. Liu Y, Wu W, Wei J, Yu Y. Visible light responsive liquid crystal polymers containing reactive moieties with good processability. ACS Appl Mat Interfaces. 2017;9:782–9.
23. Komura M, Iyoda T. AFM cross-sectional imaging of perpendicularly oriented nanocylinder structures of microphase-separated block copolymer films by crystal-like cleavage. Macromolecules. 2007;40:4106–8.
24. Komura M, Komiyama H, Nagai K, Iyoda T. Direct observation of faceted grain growth of hexagonal cylinder domains in a side chain liquid crystalline block copolymer matrix. Macromolecules. 2013;46:9013–20.
25. Tian YQ, Watanabe K, Kong XX, Abe J, Iyoda T. Synthesis, nanostructures, and functionality of amphiphilic liquid crystalline block copolymers with azobenzene moieties. Macromolecules. 2002;35:3739–47.
26. Komiyama H, Sakai R, Hadano S, Asaoka S, Kamata K, Iyoda T, Komura M, Yamada T, Yoshida H. Enormously wide range cylinder phase of liquid crystalline PEO-b-PMA(Az) block copolymer. Macromolecules. 2014;47:1777–82.
27. Komura M, Yoshitake A, Komiyama H, Iyoda T. Control of air-interface-induced perpendicular nanocylinder orientation in liquid crystal block copolymer films by a surface-covering method. Macromolecules. 2015;48:672–8.
28. Yu H, Li J, Ikeda T, Iyoda T. Macroscopic parallel nanocylinder array fabrication using a simple rubbing technique. Adv Mater. 2006;18:2213–5.
29. Wang T, Li X, Dong Z, Huang S, Yu H. Vertical orientation of nanocylinders in liquid-crystalline block copolymers directed by light. ACS Appl Mat Interfaces. 2017;9:24864–72.
30. Chen A, Komura M, Kamata K, Iyoda T. Highly ordered arrays of mesoporous silica nanorods with tunable aspect ratios from block copolymer thin films. Adv Mater. 2008;20:763–7.
31. Chen A, Zhu Q, Zhao Y, Tastumi T, Iyoda T. Novel catalysts of Au/SiO_2 hybrid nanorod arrays for the direct formation of hydrogen peroxide. Part Part Syst Char. 2013;30:489–93.
32. Li J, Kamata K, Komura M, Yamada T, Yoshida H, Iyoda T. Anisotropic ion conductivity in liquid crystalline diblock copolymer membranes with perpendicularly oriented PEO cylindrical domains. Macromolecules. 2007;40:8125–8.
33. Ikeda T, Nakano M, Yu YL, Tsutsumi O, Kanazawa A. Anisotropic bending and unbending behavior of azobenzene liquid-crystalline gels by light exposure. Adv Mater. 2003;15:201–5.
34. Qu T, Zhao Y, Li Z, Wang P, Cao S, Xu Y, Li Y, Chen A. Micropore extrusion-induced alignment transition from perpendicular to parallel of cylindrical domains in block copolymers. Nanoscale. 2016;8:3268–73.
35. White JL, Roman JF. Extrudate swell during the melt spinning of fibers influence of rheological properties and take-up force. J Appl Polym Sci. 1976;20:1005–23.
36. Bang J, Jeong U, Ryu du Y, Russell TP, Hawker CJ. Block copolymer nanolithography: translation of molecular level control to nanoscale patterns. Adv Mater. 2009;21:4769–92.
37. Ham S, Shin C, Kim E, Ryu DY, Jeong U, Russell TP, Hawker CJ. Microdomain orientation of PS-b-PMMA by controlled interfacial interactions. Macromolecules. 2008;41:6431–7.
38. Qiang Z, Zhang LH, Stein GE, Cavicchi KA, Vogt BD. Unidirectional alignment of block copolymer films induced by expansion of a permeable elastomer during solvent vapor annealing. Macromolecules. 2014;47:1109–16.
39. Jeong J, Ha JS, Lee SS, Son JG. Topcoat-assisted perpendicular and straightly parallel coexisting orientations of block copolymer films. Macromol Rapid Commun. 2015;36:1261–6.
40. Zheng X, Li Z, Zhao Y, Qu T, Cao S, Wang P, Li Y, Iyoda T, Chen A. Polydimethylsiloxane-assisted alignment transition from perpendicular to parallel of cylindrical microdomains in block copolymer films. RSC Adv. 2016;6:93298–302.